

Principled Design and Implementation of Steerable Detectors

Julien Fageot, Virginie Uhlmann, Zsuzsanna Püspöki, Benjamin Beck, Michael Unser, Adrien Depeursinge

Abstract—We provide a complete pipeline for the detection of patterns of interest in an image. In our approach, the patterns are assumed to be adequately modeled by a known template, and are located at unknown position and orientation. We propose a continuous-domain additive image model, where the analyzed image is the sum of the template and an isotropic background signal with self-similar isotropic power-spectrum. The method is able to learn an optimal steerable filter fulfilling the SNR criterion based on one single template and background pair, that therefore strongly responds to the template, while optimally decoupling from the background model. The proposed filter then allows for a fast detection process, with the unknown orientation estimation through the use of steerability properties. In practice, the implementation requires to discretize the continuous-domain formulation on polar grids, which is performed using radial B-splines. We demonstrate the practical usefulness of our method on a variety of template approximation and pattern detection experiments.

Index Terms—steerable filters, rotation invariance, pattern detection, orientation estimation, SNR criterion, isotropic Gaussian model, radial B-splines.

I. INTRODUCTION

Pattern detection and recognition is a core task of image analysis in general [1], and of bioimage informatics in particular [2]. Patterns of interest in biomedical images (*e.g.*, vessel, elongated cells, bacteria, biomolecules) are often characterized by pronounced and characteristic directional components [3], [4]. Moreover, they can appear not only at any location in the image, but also at any orientation. It follows that the major challenge for accurate pattern detection is to develop detectors that can sense discriminative directions with invariance/equivariance to translations and local rotations. It is worth noting that, most often, no variation in terms of the scale of the pattern is expected in biomedical images and that the latter is a discriminative property [5]. For this reason, we shall consider that the sought-for patterns are all present at the same scale in the image.

This leads us to formulate the detection problem as follows. We assume that the image to analyse I can be written as

$$I = \sum_i T(\mathbf{R}_{-\theta_i}(\cdot - \mathbf{x}_i)) + S, \quad (1)$$

This project has received funding from the Swiss National Science Foundation under Grants 200020-162343/1, PZ00P2_154891, and 205320_179069.

Julien Fageot, Virginie Uhlmann, Zsuzsanna Püspöki, Benjamin Beck, and Michael Unser are with the Biomedical Imaging Group, EPFL, Lausanne, Switzerland (email: julien.fageot@epfl.ch).

Adrien Depeursinge is with the Biomedical Imaging Group, EPFL, Lausanne, Switzerland and with the MedGIFT group, Institute of Information Systems, University of Applied Sciences Western Switzerland (HES-SO), Sierre 3960, Switzerland.

with T a known template dispatched at unknown locations \mathbf{x}_i and rotated at unknown orientations θ_i , and S the background signal, modeled as a Gaussian random field. Our approach is to build a filter that allows for a convolution-based detection through the complete image, working in the Fourier domain. We use steerable filters to efficiently test any possible orientation at any position, without reconvolving the image with oriented filters. The filter is designed to be discriminative in the sense that it responds strongly to the template T , while being as insensitive as possible to the background signal S . A strong constraint is that the detection filter can be learned from one unique training example (the template T provided by the user) and from the background model (characterized by a single parameter quantifying its power-spectrum decay, as we shall describe later).

A. Comparison with Previous Works

Standard methods for pattern detection are based on hand-crafted filters, transforms and criteria (*e.g.*, Hough [6], Laplacians of Gaussians [7], Canny [8], Harris [9]). These are targeting low-level image features such as lines, blobs, edges, lines or corners but are not rich enough to model higher-level templates such as complex biomolecules or cell mitosis.

Template matching allows detecting virtually any objects modeled by a template and to find image locations minimizing a given matching distance between the template and a local image neighborhood [10] (*e.g.*, sum of absolute differences, normalized cross correlation). However, template matching methods fulfilling the above-mentioned requirements in terms of invariance/equivariance to geometric transforms are computationally intensive since matching distances must potentially be evaluated for every positions and orientations of the pattern. Several solutions were proposed to accelerate the matching process [11], [12], [13]. A notable approach to allow efficient detection across pattern orientations is to use steerable detectors [14], [15], [16], [17]. The latter allow evaluating filter responses at any orientation using a simple angular-dependent linear combination of a small number of basis elements [18], [19]. We also propose a detection method relying on steerable filters. However, many approaches based on steerability focus on the detection of polar separable patterns [14], [17], possibly relaxed with a multiscale wavelet-based approach [20]. Therefore, all these methods are adapted for a specific class of template, that is polar separable or sum of finitely many polar separable components. As we shall see, a specificity of our method is to possibly consider any square-integrable template, with no restriction on polar separability, allowing

to built detectors for any kind of patterns. In addition, the strongest limitation of template matching approaches is their inability to include image background models. For background models S with non flat power spectrum, the goal is not only to match the template of interest but also to be as insensitive as possible to the statistical variations of the background. Specifying the background signal S is therefore useful to obtain discriminative detectors reducing the number of false positives. The proposed method allows including a background model in the filter design criteria, which allows to dramatically improve the detection performance in practice and is one of the main novelty of our work.

Deep convolutional neural networks (CNN) allowed tremendous progress in biomedical image analysis [21], [22], including in pattern detection [23], [24]. CNNs are able to learn a collection of detectors as deep image operators that are invariant to translations via convolutional operations. However, CNNs have two main drawbacks, making them difficult to use when little labeled training data is available. First, in their initial formulation, CNNs do not implement built-in invariance/equivariance to local rotations in most common designs, which is often palliated using rotational data augmentation [25]. More advanced approaches exist including group equivariant and steerable CNNs [26], [27] but are not, to the best of our knowledge, designed for pattern detection. More importantly, even when incorporating geometrical invariances, CNNs need an enormous number of templates and background examples to adequately learn the deep image detectors. As an order of magnitude, CheXNet [23] allowed radiologist-level pneumonia detection on chest x-rays but only when trained on more than 100,000 labeled examples [28]. They cannot be trained on-the-fly from one or a few examples. The problem tackled in this paper, in comparison, is to detect patterns of interest based on the knowledge of a *single* example.

B. Contributions

The main contributions of the paper are summarized as follows.

- *Steerable filter design*: We define a SNR criterion for the image model (1), from which we identify the optimal steerable filter for pattern detection. When the background has a flat power-spectrum (white noise model), the filter is the steerable function matching the template T (Theorem II-D). We also consider a richer background model for self-similar and isotropic power-spectrum, for which we also identify the optimal steerable filter (Proposition 2).
- *Radial B-spline expansion*: The optimal steerable filter is characterized by its Fourier domain angular/radial decomposition. The angular dependency is controlled by the use of steerable filters, which is equivalent to an angular low-pass approximation of the optimal filter. The discrete radial profile of the optimal filter is captured by developing an interpolation method based on radial B-splines, relying on the identification of the optimal B-spline-based steerable filter in Theorem III-B.
- *A complete detection algorithm*: The previous formulation allows for a practical implementation to design

steerable filter. We also provide a complete algorithm for the detection process, that we carefully evaluate experimentally.

The paper is structured in the following way. The continuous-domain theory of SNR-based optimal steerable filter design is presented in Section II. The implementation of the proposed theory on discretized image grids and detection algorithm are detailed in Section III. In Section IV, we investigate the performance and parameter sensitivity of the proposed framework. Discussions and conclusions are presented in Section V.

II. OPTIMAL STEERABLE FILTERS: THEORY

This section is dedicated to our continuous-domain framework for the detection problem. After introducing the main notations in Section II-A, we present the SNR criterion for which the optimal detectors will be constructed in Section II-B. One challenging aspect of the detection is that the pattern can be found at an unknown orientation. We address this problem by using steerable filters, introduced in Section II-C. The main theoretical result of this paper is Theorem 1 in Section II-D, which gives the formula for the optimal steerable detector considering the SNR criterion. In Section II-E, we present a refinement of this result for a richer class of background models that appears to be much more realistic than the white noise model in practice. Finally, we show how to define response maps based on the optimal detector, that can be used for the detection procedure in Section II-F.

A. Notations

Vectors in the plane are denoted in spatial domain by $\mathbf{x} = (x_1, x_2)$ and in Fourier domain by $\boldsymbol{\omega} = (\omega_1, \omega_2)$. We write (r, θ) for the polar coordinates in Fourier domain where $r \geq 0$ and $\theta \in [0, 2\pi)$. We switch from Cartesian to polar coordinates according to $(\omega_1, \omega_2) = (r \cos \theta, r \sin \theta)$ and $(r, \theta) = ((\omega_1^2 + \omega_2^2)^{1/2}, \arctan(\omega_2/\omega_1))$.

We consider functions f from \mathbb{R}^2 to \mathbb{R} . The Fourier transform of f is \hat{f} . A function f is square integrable and denoted by $f \in L_2(\mathbb{R}^2)$ if $\|f\|_2^2 = \int_{\mathbb{R}^2} |f(\mathbf{x})|^2 d\mathbf{x} < \infty$. We shall use repeatedly the Parseval relation $\langle f, g \rangle = \frac{1}{2\pi} \langle \hat{f}, \hat{g} \rangle$. The usual scalar product between two square integrable functions in Fourier domain is then

$$\langle \hat{f}, \hat{g} \rangle = \int_{\mathbb{R}^2} \hat{f}(\boldsymbol{\omega}) \overline{\hat{g}(\boldsymbol{\omega})} d\boldsymbol{\omega} = \int_0^{2\pi} \int_0^\infty \hat{f}(r, \theta) \overline{\hat{g}(r, \theta)} r dr d\theta.$$

The rotation matrix of angle α is $\mathbf{R}_\alpha = \begin{pmatrix} \cos \alpha & -\sin \alpha \\ \sin \alpha & \cos \alpha \end{pmatrix}$. Finally, $f \propto g$ means that the two functions f and g are proportional.

B. SNR Criterion for Template Approximation

We start by assuming that the image I_0 is the sum of a template of interest T and a background image S as

$$I_0(\mathbf{x}) = T(\mathbf{x}) + S(\mathbf{x}). \quad (2)$$

Mathematically, $T \in L_2(\mathbb{R}^2)$ is a square-integrable function and S is modeled as a Gaussian field with zero mean. We

call (2) the local image model, for which we have only one template localized in the center of the image. The goal is to design detection filters f that

- strongly responds to the foreground template T ,
- responds as little as possible to the background signal S , and
- can be used efficiently to determine the orientation of the template T when it is unknown.

The third requirement will be achieved by using *steerable* filters (see Section II-C below). To tackle the two first point, we want f to maximizes the *signal-to-noise ratio* (SNR), defined as

$$\text{SNR}(f) = \frac{\mathbb{E}[\langle I_0, f \rangle]^2}{\text{Var}(\langle I_0, f \rangle)}, \quad (3)$$

which is a very classical criterion in detection theory [29]. The template T is deterministic and the background signal has zero mean, we therefore have that $\mathbb{E}[\langle I_0, f \rangle] = \langle T, f \rangle$ and $\text{Var}(\langle I, f \rangle) = \text{Var}(\langle S, f \rangle)$.

C. Steerable Filters and their Fourier Radial Profiles

We aim at detecting patterns whose orientations are *a priori* unknown in an image. This can be performed using steerable filters, which can be rotated efficiently [19].

Definition 1: A filter f is *steerable* if the span of its rotated versions $f(\mathbf{R}_\alpha \mathbf{x})$, with $\alpha \in [0, 2\pi)$, is a finite-dimensional subspace of $L_2(\mathbb{R}^2)$.

The main advantage of steerable filters is that their rotation by an arbitrary angle is reduced to a finite dimensional algebraic problem. In Proposition 1, we characterize steerable filters from their polar decomposition in terms of the circular harmonic functions $\theta \mapsto e^{jn\theta}$, where $n \in \mathbb{Z}$.

Proposition 1: A function $f \in L_2(\mathbb{R}^2)$ can be uniquely decomposed in polar coordinates in Fourier domain as

$$\widehat{f}(r, \theta) = \sum_{n \in \mathbb{Z}} \widehat{f}_n(r) e^{jn\theta}, \quad (4)$$

where the \widehat{f}_n jointly satisfy $\sum_{n \in \mathbb{Z}} \|\widehat{f}_n\|_2^2 < \infty$. The functions \widehat{f}_n , called the *Fourier radial profiles* of f , are given by

$$\widehat{f}_n(r) = \frac{1}{2\pi} \int_0^{2\pi} \widehat{f}(r, \theta) e^{-jn\theta} d\theta. \quad (5)$$

Moreover, f is steerable if and only if finitely many \widehat{f}_n are non-zero.

The proof of Proposition 1 is presented in Appendix B. As a consequence, the general form of a steerable filter in the Fourier domain is $\widehat{f}(r, \theta) = \sum_{n \in H} \widehat{f}_n(r) e^{jn\theta}$, where H is a finite subset of \mathbb{Z} and $\widehat{f}_n \in L_2(\mathbb{R}^2)$ the non zero Fourier radial profiles. We have in that case that

$$\widehat{f(\mathbf{R}_\alpha \cdot)}(\omega) = \widehat{f}(\mathbf{R}_\alpha \omega) = \widehat{f}(r, \theta + \alpha) = \sum_{n \in H} e^{jn\alpha} \widehat{f}_n(r) e^{jn\theta}. \quad (6)$$

Hence, any rotated version of f is a linear combination of the inverse Fourier transforms of the $\widehat{f}_n(r) e^{jn\theta}$ for $n \in H$, meaning that f is steerable in the sense of Definition 1.

Finally, any function f can be approximated by steerable functions at an arbitrary precision. Indeed, it is sufficient to consider the truncated sums $\sum_{|n| \leq N} \widehat{f}_n(r) e^{jn\theta}$ that converge to \widehat{f} in $L_2(\mathbb{R}^2)$ when the number of harmonics N increases.

D. Optimal Steerable Filter Learning for White Background

In this section, we assume that the background signal S is a Gaussian white noise, which corresponds to a flat power spectrum. This implies that $\text{Var}(\langle S, f \rangle) = \sigma^2 \|f\|_2^2$, with σ^2 the variance of S (see Appendix A). As a consequence, (3) becomes

$$\text{SNR}(f) = \frac{1}{\sigma^2} \frac{|\langle T, f \rangle|^2}{\|f\|_2^2} = \frac{1}{\sigma^2} \frac{|\langle \widehat{T}, \widehat{f} \rangle|^2}{\|\widehat{f}\|_2^2}, \quad (7)$$

where we used the Parseval relation for the Fourier domain expression. Note that the SNR is well-defined for any square-integrable filter, due to the assumption that $T \in L_2(\mathbb{R}^2)$. In Section II-E, we will also consider more evolved background models.

For a given finite set of harmonics H , it is then possible to specify the optimal steerable filter for the SNR criterion (7) associated to the image model (2).

Theorem 1: A filter f maximizes the SNR criterion (7) among the space of steerable filters with harmonics in H if and only if

$$\widehat{f}(r, \theta) \propto \sum_{n \in H} \widehat{T}_n(r) e^{jn\theta}, \quad (8)$$

with \widehat{T}_n the Fourier radial profiles of T given for each harmonic n by

$$\widehat{T}_n(r) = \frac{1}{2\pi} \int_0^{2\pi} \widehat{T}(r, \theta) e^{-jn\theta} d\theta. \quad (9)$$

The optimal filter is defined up to a multiplicative constant since $\text{SNR}(\lambda f) = \text{SNR}(f)$ for every scalar $\lambda \neq 0$. The proof of Theorem 1 is given in Appendix C. The optimal filter is completely determined by the template to approximate T and the set of harmonics H . In practice, the main issue is to compute the integral (9) while knowing only T on a finite cartesian grid in the Fourier domain. This point will be discussed extensively in Section III.

E. Isotropic Self-similar Background Model and Whitening

The SNR criterion (7) is based on the assumption that the background is adequately modeled as a Gaussian white noise, corresponding to the case where its power spectrum $P_S(\omega)$ is nearly constant. In this section, we consider a richer model for the background signal. Indeed, it has been shown in many signal and image processing applications that the power spectrum of the signal of interest follows a power law [30], [31], [32], [33], [20], and is therefore smoother than a white noise. We moreover make the assumption that the background

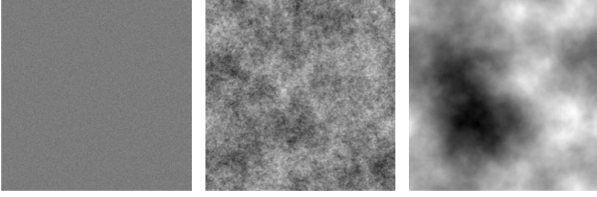


Fig. 1. Realizations of ISS Gaussian fields for different values of γ . From left to right: $\gamma = 0$ (white noise), $\gamma = 1$, $\gamma = 2$.

is statistically isotropic, which is equivalent to saying that the power spectrum is a radial function $P_S(\boldsymbol{\omega}) = P_S(r)$.

Mathematically, this means that the background signal satisfies the equation

$$(-\Delta)^{\gamma/2} S = W \quad (10)$$

with W a Gaussian white noise and $(-\Delta)^{\gamma/2}$ the fractional Laplacian of order $\gamma \geq 0$. Then, the background signal S is an *isotropic self-similar (ISS) Gaussian field* [34], [35]. In this case, S can be *whitened*, in the sense that it can be linearly transformed into a white noise. This is what we refer to as background model “with whitening”.

We call γ the *self-similarity parameter* of S . It plays a crucial role in determining the smoothness properties of the background model. The power spectrum of S is then $P_S(\boldsymbol{\omega}) = P_S(r) = \sigma^2/r^{2\gamma}$, with σ^2 the variance of the underlying white noise. As a consequence, the higher γ , the smoother S . For illustration purposes, we represent several ISS Gaussian fields in Figure 1.

We now establish the general implications of this background model. More technical details can be found in Appendix A. First, we shall consider filters such that $\langle S, f \rangle$ is well-defined, which requires that $(-\Delta)^{\gamma/2} g = f$ for some $g \in L_2(\mathbb{R}^2)$, or equivalently, $\hat{f}(\boldsymbol{\omega})/\|\boldsymbol{\omega}\|^\gamma \in L_2(\mathbb{R}^2)$. Then, $\langle S, f \rangle$ is a well-defined Gaussian random variable with zero mean and variance

$$\text{Var}(\langle S, f \rangle) = \frac{\sigma^2}{2\pi} \int_0^\infty r^{1-2\gamma} \int_0^{2\pi} |\hat{f}(r, \theta)|^2 d\theta dr \quad (11)$$

as shown in Appendix (A).

Finally, the SNR criterion (3) becomes, for this background model,

$$\text{SNR}(f) = \frac{1}{\sigma^2} \frac{|\langle \hat{T}, \hat{f} \rangle|^2}{\|\hat{g}\|_2^2}. \quad (12)$$

We now present how to maximize this new criterion.

Proposition 2: A steerable filter f with finite set of harmonics H maximizes the SNR criterion (12) for the self-similarity order $\gamma \geq 0$ if and only if

$$\hat{f}(r, \theta) \propto r^{2\gamma} \sum_{n \in H} \hat{T}_n(r) e^{jn\theta}, \quad (13)$$

where \hat{T}_n are the Fourier radial profiles of T given by (9).

Proposition 2 is proved in Appendix D. The effect of the whitening is a multiplication in the Fourier domain of the optimal filter for the SNR criterion (8) by $r^{2\gamma}$.

In practice, we do not necessarily know the self-similar parameter. We can nevertheless estimate γ from the background signal S itself. The principle is as follows. For a test function f and a scale $a > 0$, we consider $a^{-1}f(\cdot/a)$ whose L_2 -norm does not depend on a and which allows analyzing the background signal S at scale a . Then, the variance of $X_a = \langle S, a^{-1}f(\cdot/a) \rangle$ is known to be proportional to $a^{2\gamma}$ [36, Proposition 5.6]. We therefore perform a multiscale analysis at various $a > 0$ to estimate the parameter γ from the theoretical linear relation between $\log \text{Var}(X_a)$ and $\log a$, namely

$$\log \langle S, a^{-1}f(\cdot/a) \rangle = 2\gamma \log a + b, \quad (14)$$

where $b \in \mathbb{R}$. This method has been implemented to analyse the statistics of natural images in [36] and found to be robust.

Finally, we remark that one may have only access to $I_0 = T + S$ in (2), and not to the template T itself, to design the optimal steerable filter. In that case, one can use background subtraction techniques to recover T from I_0 . We do not discuss this aspect further in the paper and we assume to have access to a good template representation.

F. Detection Procedure

The objective of the detection process is to reveal the positions and orientations of patterns corresponding to a template $T(\boldsymbol{x})$ in a (larger) image $I(\boldsymbol{x})$. We model I as a sum of templates of interest T_i , positioned at locations \boldsymbol{x}_i and rotated with an angle θ_i , and a background image S . Mathematically, I is therefore a function from \mathbb{R}^2 to \mathbb{R} such that

$$I(\boldsymbol{x}) = \sum_i T(\mathbf{R}_{-\theta_i}(\boldsymbol{x} - \boldsymbol{x}_i)) + S(\boldsymbol{x}), \quad (15)$$

with $T \in L_2(\mathbb{R}^2)$, $\boldsymbol{x}_i \in \mathbb{R}^2$, $\theta_i \in [0, 2\pi)$, and S is an ISS Gaussian field. Here, we assume that the template T and the variance of the background signal S are known, while the \boldsymbol{x}_i and θ_i are unknown. In order to detect template locations \boldsymbol{x}_i at the correct orientations θ_i , we can efficiently compute the two following quantities using the steerability property (6) of our detector f as

$$I_{\text{ang}}(\boldsymbol{x}_0) = \arg \max_{\theta_0} \langle I(\cdot - \boldsymbol{x}_0), f(\mathbf{R}_{\theta_0} \cdot) \rangle, \quad (16)$$

$$I_{\text{amp}}(\boldsymbol{x}_0) = \max_{\theta_0} \langle I(\cdot - \boldsymbol{x}_0), f(\mathbf{R}_{\theta_0} \cdot) \rangle \\ = \langle I(\cdot - \boldsymbol{x}_0), f(\mathbf{R}_{I_{\text{ang}}(\boldsymbol{x}_0)} \cdot) \rangle, \quad (17)$$

where $I_{\text{ang}}(\boldsymbol{x}_0)$ is the estimated orientation of T at $\boldsymbol{x}_0 \in \mathbb{R}^2$ and $I_{\text{amp}}(\boldsymbol{x}_0)$ is the amplitude of the maximum response of f at \boldsymbol{x}_0 . It is worth noting that $I_{\text{amp}}(\boldsymbol{x}_i)$ will be maximized when $I_{\text{ang}}(\boldsymbol{x}_i) \approx \theta_i$.

III. OPTIMAL STEERABLE FILTERS: DISCRETIZATION

We have now described how to deduce the optimal steerable filter associated to a template T in a background signal S . The formulation of Section II is in the continuous-domain, although images are in practice stored as discrete arrays in a computer. The concrete design of detection algorithms therefore requires the discretization of the proposed theory.

Practically, one should compute the optimal steerable detector f in (8) from a discretized version of the template of

interest T . Computing f requires an angular averaging over the Fourier transform of the template in (9). The approximation of (9) on the Cartesian grid is challenging because it involves evaluating integrals over the angular polar coordinate θ for all values of r , where much less samples are available when r is small.

The discretization we propose essentially relies on the expansion of the Fourier radial profiles in terms of radial B-splines, the latter being introduced in Section III-A. We then combine the circular harmonics and the radial B-splines in Section III-B, and obtain the discretized optimal steerable filter in Theorem 2. Finally, we summarize how to compute the discretized version of the optimal steerable filter in Section III-C.

A. B-Spline Expansion of the Radial Profiles

Cardinal B-splines are well-known for the capability of approximating continuous-domain functions based on discrete measurements [37]. The theory is traditionally developed for one-dimensional functions from \mathbb{R} to \mathbb{R} , and has to be slightly modified in our context, since we deal with *radial* functions.

The B-spline of degree 0 is $\beta_0(x) = 1_{[0,1]}(x)$. The spline of degree $(M + 1)$ is defined recursively as $\beta_{M+1}(x) = \beta_M * \beta_0(x)$. In our experiments, we use the quadratic B-spline β_2 , which is supported over $[0, 3]$ and is piecewise quadratic on the intervals $[k, k + 1]$, $k \in \mathbb{Z}$. The closed form expression of the quadratic spline can be found for instance in [38]. Thereafter, we write $\beta_2 = \beta$ to simplify the notation.

1) *Radial B-splines:* A radial B-spline is a radial function $\hat{f}(r)$ in $L_2(\mathbb{R}^2)$ of the form

$$\hat{f}(r) = \sum_{k \in \mathbb{Z}} \frac{c[k]}{r_0} \beta \left(\frac{r}{r_0} - k \right), \quad (18)$$

with $r_0 > 0$ the discretization step and $c[k]$ the spline coefficients of \hat{f} . The function \hat{f} is defined for radius $r \geq 0$. One could therefore restrict the sum in (18) to integers k such that the support of $\beta(\cdot/r_0 - k)$ intersects \mathbb{R}^+ . For quadratic splines, this corresponds to $k \geq -2$. However, we prefer to keep the summation over all integers, allowing to consider discrete convolutions between sequences indexed by $k \in \mathbb{Z}$. In what follows, we approximate the Fourier radial profiles of the template T using radial B-splines.

2) *Approximation with Radial B-Splines:* A radial function $\hat{f} \in L_2(\mathbb{R}^2)$ can be approximated by radial B-splines of the form (18) at arbitrary precision by taking the discretization step $r_0 \rightarrow 0$. This is well-known for classical B-splines [38] and can be adapted to the case of radial B-splines.

The main difference between the usual B-splines expansion of 1D functions and the B-spline expansion of 2D radial functions is that one changes the scalar product. We recall that the 2D scalar product between two radial functions \hat{f} and \hat{g} is given by

$$\langle \hat{f}, \hat{g} \rangle = \int_0^\infty \int_0^{2\pi} \hat{f}(r) \overline{\hat{g}(r)} r d\theta dr = 2\pi \int_0^\infty \hat{f}(r) \overline{\hat{g}(r)} r dr.$$

To facilitate computations, we identify a radial function $\hat{f} : \mathbb{R}^+ \mapsto \mathbb{C}$ to its symmetrization $\hat{f} : \mathbb{R} \mapsto \mathbb{C}$ such that $\hat{f}(-r) = \hat{f}(r)$. In particular, the scalar product between two radial functions becomes $\langle \hat{f}, \hat{g} \rangle = \pi \int_{\mathbb{R}} \hat{f}(r) \overline{\hat{g}(r)} |r| dr$. All the scalar products between radial functions have to be understood with this symmetrization procedure.

The expansion of a radial function in the quadratic spline basis requires special attention since the family is not orthogonal. We can overcome this using classical techniques for B-splines that we adapt to the case of radial B-splines. We set $h[k] = \langle \beta, \beta(\cdot - k) \rangle$ for each $k \in \mathbb{Z}$. The filter h is nonzero only for $|k| \leq 2$ due to the support of β . The fact that h differs from the Kronecker δ means precisely that the family of shifted B-spline is not orthonormal. Since g is compactly supported, there exists a unique discrete filter $h^{-1} = (h^{-1}[k])_{k \in \mathbb{Z}}$ such that $(h * h^{-1})[k] = (h^{-1} * h)[k] = \delta[k]$ [39], [40]. Then, h^{-1} plays a crucial role to accurately identify the optimal B-spline coefficients to approximate a radial function.

For any radial function $\hat{f} \in L_2(\mathbb{R}^2)$, its projection to the space of radial B-splines with discretization step r_0 is denoted by

$$P_{r_0}\{\hat{f}\}(r) = \sum_{k \in \mathbb{Z}} \frac{c[k]}{r_0} \beta \left(\frac{r}{r_0} - k \right), \quad (19)$$

Proposition 3: Let $f \in L_2(\mathbb{R}^2)$. For $k \in \mathbb{Z}$, we set

$$d[k] = \frac{1}{2\pi} \left\langle \hat{f}(r, \theta), \frac{1}{r_0} \beta \left(\frac{r}{r_0} - k \right) \right\rangle. \quad (20)$$

Then, the coefficients in the orthogonal projection (3) of \hat{f} are computed as

$$c[k] = (h^{-1} * d)[k]. \quad (21)$$

Proposition 3 is proved in Appendix E. It gives the optimal approximation of a radial function in terms of radial B-splines for a given discretization step. Note that the discrete filter h^{-1} does not depend on the discretization step r_0 .

B. Combining Radial B-splines and Circular Harmonics

We define the family of functions $\varphi_{n,k}$, $n, k \in \mathbb{Z}$, given in the Fourier domain by

$$\hat{\varphi}_{n,k}(r, \theta) = \frac{1}{r_0} \beta \left(\frac{r}{r_0} - k \right) e^{jn\theta}. \quad (22)$$

For a fixed finite set of harmonics $H \subset \mathbb{Z}$ and discretization step $r_0 > 0$, one denotes by $P_{r_0, H}\{\hat{f}\}$ the orthogonal projection of the function \hat{f} onto the space generated by the $\hat{\varphi}_{n,k}$ for $n \in H, k \in \mathbb{Z}$.

We can combine Proposition 1 and Proposition 3 to approximate any square-integrable function by steerable functions whose Fourier radial profiles are B-splines.

Theorem 2: Let $r_0 > 0$ and $H \subset \mathbb{Z}$. For any function $T \in L_2(\mathbb{R}^2)$, the orthogonal projection of its Fourier transform on the $\hat{\varphi}_{n,k}$, $n \in H, k \in \mathbb{Z}$ is

$$P_{r_0, H}\{\hat{T}\}(r, \theta) = \sum_{n \in H} \sum_{k \in \mathbb{Z}} c_n[k] \hat{\varphi}_{n,k}(r, \theta), \quad (23)$$

where $c_n[k] = (h^{-1} * d_n)[k] = \sum_{\ell \in \mathbb{Z}} h^{-1}[\ell] d_n[k - \ell]$ and

$$d_n[k] = \frac{1}{2\pi} \left\langle \widehat{T}, \varphi_{n,k} \right\rangle = \frac{1}{2\pi} \left\langle \widehat{T}_n(r), \frac{1}{r_0} \beta \left(\frac{r}{r_0} - k \right) \right\rangle. \quad (24)$$

Moreover, when $r_0 \rightarrow 0$ and $H \rightarrow \mathbb{Z}$, the orthogonal projection converges to any T for the L_2 -norm.

Theorem 2 is proved in Appendix E. It allows to compute an approximation of any template T from the B-spline coefficients $c_n[k]$ of the n th radial profile for each n . Moreover, this approximation can be as good as required by diminishing the step size r_0 and increasing the number of harmonics. These coefficients are obtained via the $d_n[k]$, computing a simple convolution. Note that this operation is necessary because the family $\varphi_{n,k}$ is not orthogonal. In practice, one obtains the coefficients $d_n[k]$, and therefore $c_n[k]$, by computing scalar products of the form (24).

Theorem 2 means that one can approximate the optimal steerable filter based on the integral (24). This is a clear improvement since this 2D integral can be approximated from the knowledge of T on a finite Cartesian grid. We develop this last point in the next section.

C. Computing the Discretized Optimal Steerable Detector

In practice, we have access to the template T in a finite square grid. The steps to compute the optimal steerable detector in Theorem 1 are as follows.

- Fix the set of harmonics H and the discretization step r_0 .
- Compute the discrete Fourier transform \widehat{T} of T via fast Fourier transform (FFT).
- Compute the coefficients $d_n[k]$ for $n \in H$ and $k \in K$, where K is the set of integers such that $r_0 k$ remains in the range of the image. To do so, we note that the scalar product (24) is expressed as an integral in Cartesian coordinates as

$$d_n[k] = \int_{\mathbb{R}^2} \widehat{T}(\omega_x, \omega_y) \widehat{\varphi}_{n,k}(\omega_x, \omega_y) d\omega_x d\omega_y. \quad (25)$$

This integral is approximated with its Riemann sum, from the knowledge of \widehat{T} on the Cartesian grid. The expression of the basis functions $\widehat{\varphi}_{n,k}$ in Cartesian coordinates is

$$\widehat{\varphi}_{n,k}(\omega_x, \omega_y) = \frac{1}{r_0} \beta \left(\frac{\sqrt{\omega_x^2 + \omega_y^2}}{r_0} - k \right) e^{jn \arctan(\omega_y/\omega_x)}. \quad (26)$$

- For every $n \in H$ and $k \in K$, we compute the $c_n[k]$ according to $c_n[k] = (h^{-1} * d_n)[k]$.
- Finally, the optimal spline-based steerable filter f_{opt} is given in the Fourier domain by

$$\widehat{f}_{\text{opt}}(r, \theta) = \sum_{k \in K} \sum_{n \in H} c_n[k] \frac{1}{r_0} \beta(r/r_0 - k) e^{jn\theta}. \quad (27)$$

We remark that the Riemann sum approximating the integral (25) is obtained from a finite number of coefficients only. Indeed, it deals with the grid points lying in the area delineated by the radial function $\beta(r/r_0 - k)$. When the template is known only on a coarse grid, the quality of the estimation of

$d_n[k]$ can therefore be insufficient. We remedy to this issue by zero-padding the template T in space domain to increase the size of the image. This corresponds to a sinc interpolation in Fourier domain, increasing the number of points on which the integral (25) is computed. The relevance of our discretization method for the construction of the optimal steerable detector is investigated and illustrated in Section IV.

When the background signal S is adequately modeled as an ISS Gaussian field of self-similar parameter γ (see Section II-E), the optimal detector is characterized in Proposition 2. It is simply obtained by multiplying (27) with $r^{2\gamma}$. We recall that the estimation of γ can be performed efficiently on a single realization of the background S using the method developed in [36].

IV. RESULTS

In this section, we evaluate the performance and parameter sensitivity of the proposed optimal steerable filter design. We first focus on template approximation, and follow with pattern detection and orientation estimation.

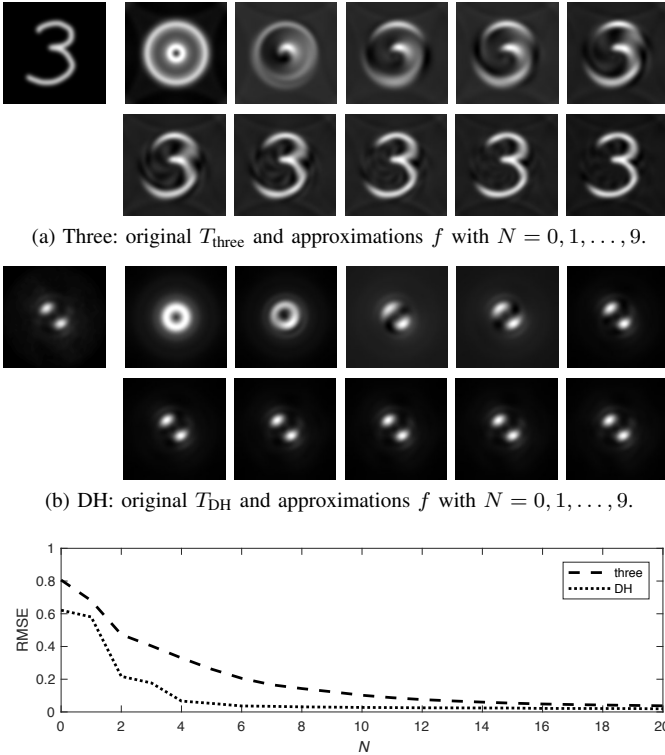
A. Template Approximation

We first evaluate the template approximation ability of the proposed SNR-based filter design criterion under the hypothesis of Gaussian white noise (Theorem 1). The optimal steerable detector is computed following the steps described in Section III-C. Both qualitative and quantitative results are showed in Figure 2 for a template containing (a) a hand-drawn “three” T_{three} and (b) T_{DH} , a double helix (DH) point spread function [41]. The approximation performance is measured in terms of root mean squared error (RMSE). The dimensions of the templates are 200×200 . The parameter r_0 in (27) is determined for each template independently as a trade-off between achieving a fine-grained resolution for the interpolation of r as well as having a sufficient number of coefficients in the Riemann sum approximating the integral (25). In all experiments, r_0 of 0.033 and 0.041 were used for T_{three} and T_{DH} , respectively.

Figure 2 shows that although using more harmonics consistently reduces the approximation error, only a small number of harmonics (*e.g.*, $N \approx 6$) is required to achieve accurate template modeling. Such a small amount of harmonics yields a low-pass approximation of the templates in terms of circular frequencies, which is striking for T_{three} (see Figure 2 (a)). For T_{DH} , the decrease of RMSE with N is less regular, where the second harmonic is of paramount importance to model the two characteristic diametrically opposed blobs of the DH. The decrease of RMSE is much faster for T_{DH} , which is circularly smoother than T_{three} . We observe in Figure 2 (c) that Fourier based approximation are better-suited for regular patterns.

B. Detection: Position and Orientation Estimation

The images are generated following the mathematical model (15). To evaluate the relevance of the proposed quantities for detection, we use semi-controlled experimental conditions by randomly positioning and orienting several occurrences of a



(a) Three: original T_{three} and approximations f with $N = 0, 1, \dots, 9$.
 (b) DH: original T_{DH} and approximations f with $N = 0, 1, \dots, 9$.
 (c) Evolution of template approximation error (RMSE) with respect to N .
 Fig. 2. Influence of the number of harmonics N for template approximation.

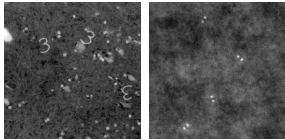


Fig. 3. Semi-controlled experimental conditions for evaluating the detection performance. Left: T_{three} in histopathological background (1200×1200). Right: T_{DH} in an ISS Gaussian field (1200×1200 , $\gamma = 1.2$).

template T added to the background S to form the image I containing S with a controlled noise level σ . We aim at estimating the template locations x_i together with their orientation θ_i . The orientation is estimated according to (16), while the amplitude of the maximum response of the filter f at x_0 , defined in (17), is used as our detection score in the following experiments.

We consider the templates from Figure 2, where T_{three} and T_{DH} are blended into various portions of histopathological images¹ and distinct realizations of ISS Gaussian fields ($\gamma = 1.2$), respectively (Figure 3).

We evaluate the position detection performance using precision-recall (PR) as well as receiver operating characteristic (ROC) analysis based on pixelwise scores from every positions in I_{amp} and angles I_{ang} . We use a severe detection criteria where only the unique pixel corresponding to the center of the template is considered a true positive. Since the ratio of true positives over true negatives is very small in this setting (e.g., $1/500,000$), ROC analysis is used to focus

¹4422 \times 2934 image of *plasmodium falciparum*, courtesy of Dr. M. D. Hicklin, public domain.

on the ability of the system to find the true positions of the template, whereas PR curves better reveal the system trend to generate false detections. All experiments compare areas under the PR or ROC curve (AUC) when assuming that the background signal is either a white noise that does not require any whitening process (referred to as “no whitening”) or a ISS Gaussian field whose self-similar parameter γ is estimated (referred to as “whitening”).

We explore the parameter sensitivity of the proposed approach in the following paragraphs. Unless specifically studied, the parameters were fixed to a noise level of $\sigma = 1$ and $M = 30$ tested angles in $[0, 2\pi)$. The estimated whitening parameters γ were of 1.35 and 1.21 for the histopathological images and the ISS Gaussian fields, respectively. The latter were estimated using the method described in the last paragraph of Section III-C and was based on 10 realizations of $S(x)$. The number N of harmonics used to approximate the template were 20 and 8 for the T_{three} and T_{DH} , respectively.

The robustness of detection performance for various noise levels is first investigated in Figure 4 for T_{three} . The use of whitening allows excellent robustness to noise, where an average ROC AUC of 0.98 and an angular error below 10 degrees are observed for a noise level $\sigma = 5$ (the template can be hardly seen with such a noise variance). This highlights the adequacy of the fractional Laplacian model for the histopathological background. The evolution of the PR AUC and the corresponding cropped response maps suggest that most false positives occur in the vicinity of the true position. The resulting false positive can subsequently be ruled out by enforcing a minimum distance between distinct detections. A performance comparison based on a Laplacian of Gaussian (LoG) filter with optimized scale $\sigma_{\text{LoG}} \in [5, 100]$ (with a step of 5) is provided as a baseline. The LoG is a zero-mean band-pass handcrafted filter that is standard in several image analysis algorithms involving detection (e.g., scale-invariant feature transform (SIFT) [42], scale-space analysis [43], Marr’s theory on vision and detection [7]). We observe that the detection performance obtained with the latter is very low and highlights the difficulty of the task when the considered templates are not isotropic and entangled in complex backgrounds. Similar trends were observed for T_{DH} in Figure 4. The importance of the whitening operation is even more striking, which is explained by the fact that the background noise is the realization of an ISS Gaussian fields.

The robustness of the estimation of the whitening parameter γ and its influence on the detection performance is studied in Table I and Figure 6. The estimated values $\tilde{\gamma}$ are found to be robust to the presence of templates for both types of background noise, which suggests that the whitening parameter can be directly estimated from $I(x)$ when the template density is relatively low. A value of $\tilde{\gamma} = 1.2$ corresponds to the ground truth for ISS Gaussian fields. The optimal values for detection for T_{three} and T_{DH} were $\gamma_{\text{opt}} = 1.2$ and $\gamma_{\text{opt}} = 1.4$, respectively, which are close to $\tilde{\gamma}$. Even if the correspondence between $\tilde{\gamma}$ and γ_{opt} is remarkable, a precise estimation of γ is not found to be critical as the PR AUC plateaus around γ_{opt} . It is worth noting in Figure 6 that in the case of detecting T_{DH} in the ISS Gaussian field, the assumption of white background

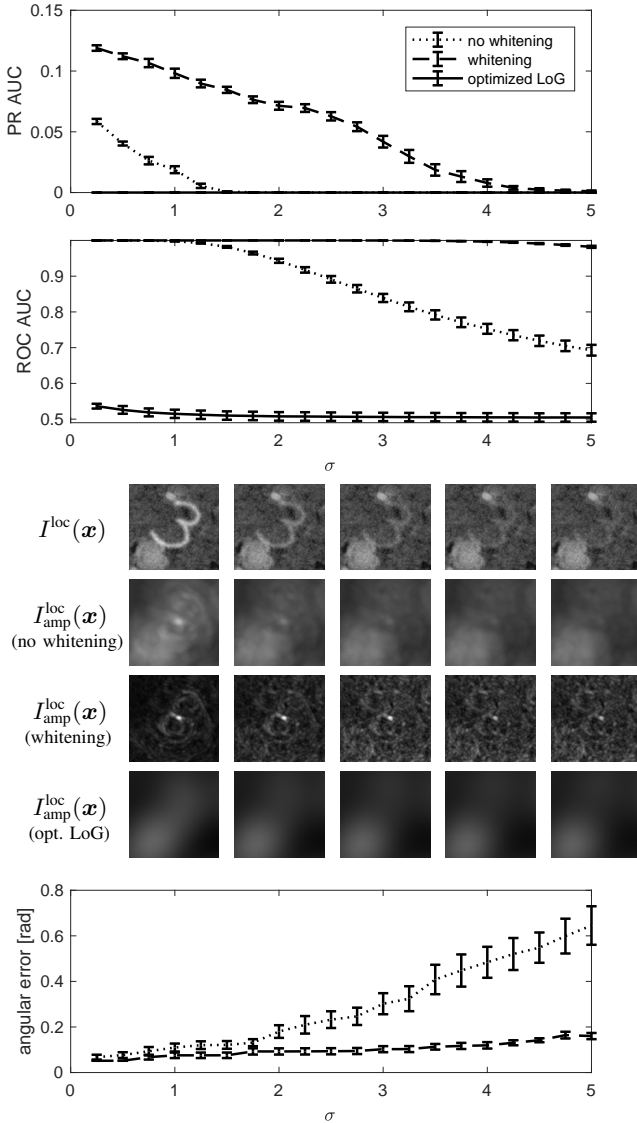


Fig. 4. Robustness of detection of T_{three} for various noise levels (histopathological background). Cropped thumbnails of the image I^{loc} , and response $I_{\text{amp}}^{\text{loc}}(\mathbf{x})$ are shown to illustrate and compare the spatial distribution of the detection scores around a true positive for the corresponding noise levels $\sigma = 1, \dots, 5$. The performance obtained with an optimized LoG filter ($\sigma_{\text{LoG}} = 60$) is reported as a baseline (it does not appear in the last plot since it is isotropic and does not allow for angle estimation).

noise (*i.e.*, no whitening) leads to poor detection performance. This is consistent with the findings in Figure 5: the whitening operation becomes essential with this type of background (ISS Gaussian fields).

The importance of the number of harmonics N for template modeling was investigated in Section IV-A. The impact of the latter on detection performance is shown in Figure 7 for T_{DH} . The observed AUC and angular errors are consistent with our previous observations, where the importance of harmonic $N = 2$ is highlighted to capture the two blobs of T_{DH} . The performance is stable for $N \geq 4$, and using more harmonics does not significantly improve the detection. Similar observations are made on the influence of N for detecting T_{three} .

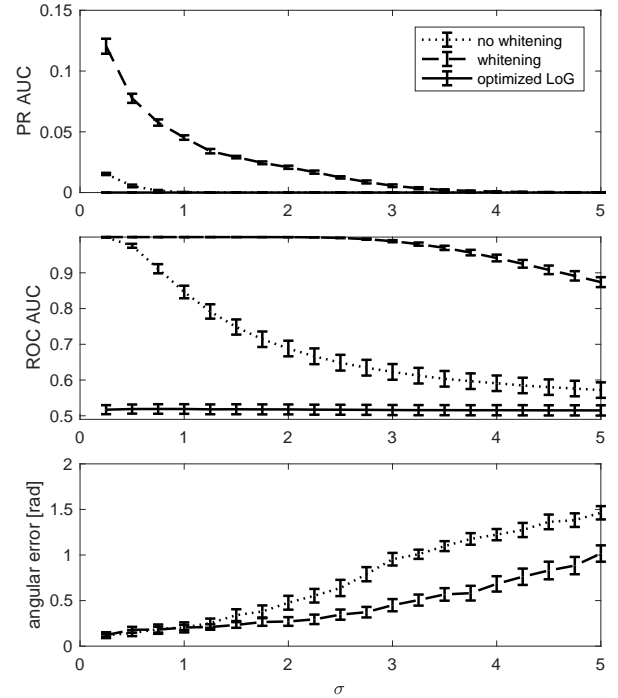


Fig. 5. Robustness of detection of T_{DH} for various noise levels (ISS Gaussian fields). The performance obtained with an optimized LoG filter ($\sigma_{\text{LoG}} = 20$) is reported as a baseline (it does not appear for the last plot).

TABLE I
ESTIMATED WHITENING PARAMETER VALUES $\tilde{\gamma}$ ARE COMPARED WHEN BASED ON THE PURE BACKGROUND $S(\mathbf{x})$ VERSUS $I(\mathbf{x})$ CONTAINING THE TEMPLATES (15). THE VALUES YIELDING OPTIMAL DETECTION PERFORMANCE γ_{opt} ARE COMPARED.

$S(\mathbf{x})$	$\tilde{\gamma}$ from $S(\mathbf{x})$	$\tilde{\gamma}$ from $I(\mathbf{x})$	γ_{opt}
ISS Gaussian fields ($\gamma = 1.2$)	1.2	1.21	1.2
histopathological images	1.31	1.35	1.4

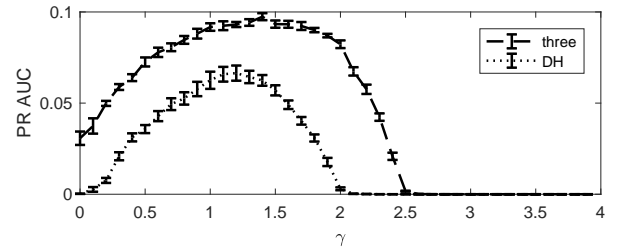


Fig. 6. Evolution PR AUC with the whitening parameter γ for T_{three} and the histopathological background as well as for T_{DH} and the ISS Gaussian field. γ_{opt} values of 1.4 and 1.2 corresponds to the optimal PR AUC for T_{three} and T_{DH} , respectively. In both cases, a precise estimation is not critical as the AUC plateaus around γ_{opt} .

Finally, the influence of the number M of tested angles in $[0, 2\pi)$ for (16) and (17) is studied in Figure 8 for T_{three} . we also report the *baseline* angular error corresponding to the sampling step π/M . Whereas the performance consistently increases with M , relatively coarse angular discretization (*e.g.*, $M = 12$) yields near to optimal detection rates. When $M \leq 7$

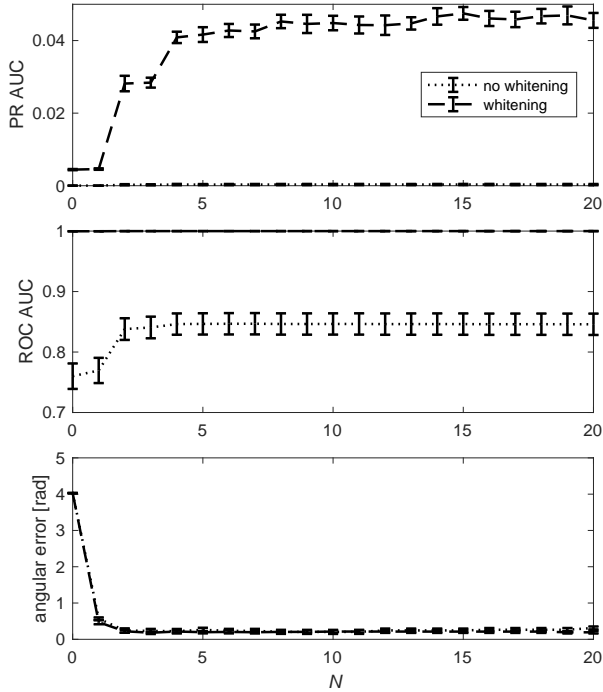


Fig. 7. Impact of the number of harmonics N on detection for T_{DH} . The findings are consistent with the study of template approximation error in Figure 2, where the second harmonic is capturing the two distinctive blobs of the DH.

the ROC AUC appears to be significantly higher for the non-whitened detector, which is contrasting with all other experiments. This may indicate that the whitened detector must be aligned with increased precision (e.g., $M \geq 10$) to provide optimal results when compared to the non-whitened one. Once again, very similar trends were observed on the influence of M for detecting T_{DH} in ISS Gaussian fields.

V. DISCUSSION AND CONCLUSION

The main goal of this paper was to provide a complete pipeline for the detection of specific patterns at unknown positions and orientations in an image. The key ingredients of our approach are (a) a continuous-domain formulation of the detection problem based on steerable filters and the optimization of the SNR criterion (Section II), (b) a B-spline based discretization scheme (Section III), and (c) an additional “whitening” procedure to extract statistical information from the background (the self-similar parameter γ) and specify an appropriate image model. We have demonstrated the abilities of our detection procedure in practice (Section IV) and estimated adequately the position and orientation of the pattern of interest. We briefly recap the main contributions of this paper.

- We approximate a template with steerable filters, which provides a low-pass approximation retaining only small angular frequencies. In practice, we have seen that only few angular frequencies are required for good template approximation (Figure 2) or pattern detection (Figure 7).
- In contrast to many other works [17], we do not construct *polar separable* steerable filters. This enables us to approximate any possible template T at arbitrary precision

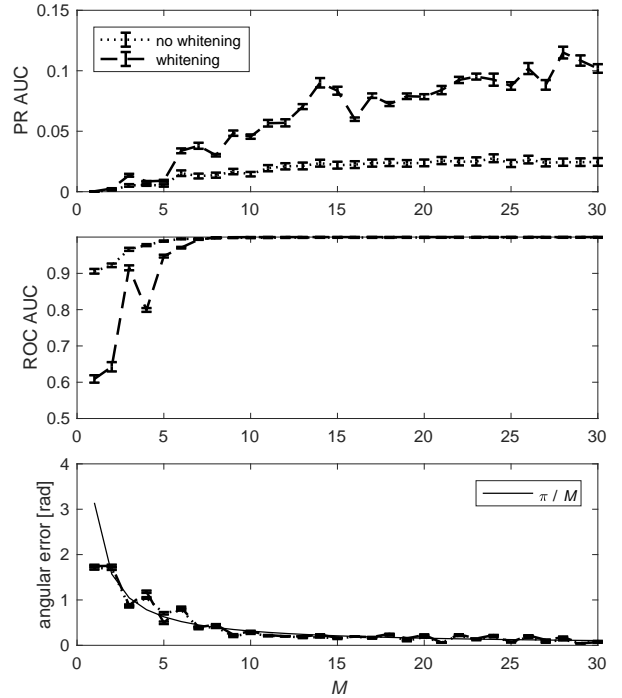


Fig. 8. Number M of angles tested in $[0, 2\pi)$ for the construction of I_{ang} and I_{amp} . The baseline angular error π/M is reported.

(Proposition 1), allowing for the precise detection of non-separable patterns such as the ones used in our experiments (three and double-helix).

- Our method lies on the assumption that the patterns of interest in the image are adequately modeled by a common template T provided by the user, as in (15). Under this assumption, we are then able to precisely detect patterns featuring occurrences of this template (Section IV-B) with a strong robustness to noise (Figure 4).
- The whitening procedure (Section II-E) tremendously improves the detection performance (Figure 6). This demonstrates the relevance of considering non-white background models. The proposed isotropic and self-similar model only requires the estimation of one parameter, γ , for which we provide a theoretically justified procedure.
- As a by-product of our method, we are not only able to recover the positions of the patterns, but also their a priori unknown orientation. This information is simply extracted from the angular map I_{ang} in (16). To refine angular accuracy, one should consider enough tested angles. Higher values of M do not significantly increase the detection performance but obviously affect the angular error (Figure 8). This additional angular information could be exploited in segmentation [44] or to extract directional features of the object of interest.

Limitations of the current approach includes the modeling of one single template per detector. However, this potential weakness is compensated by the ability of the model to approximate any template with high accuracy. In addition, a collection of detectors can be obtained by repeating the learning process

for each distinct template class. Detection robustness with respect to pattern deformations was not specifically evaluated. Nevertheless, we believe that using steerable models with a small number of harmonics results in regularized (i.e., low-pass) detectors capturing the global layout of the template with enhanced generalization abilities.

APPENDIX

A. Gaussian Models for Background Signals

A two-dimensional Gaussian field $S : \mathbb{R}^2 \rightarrow \mathbb{R}$ is such that $\langle S, f \rangle = \int_{\mathbb{R}^2} S(\mathbf{x})f(\mathbf{x})d\mathbf{x}$ is Gaussian for every test function f . The Gaussian white noise W is probably the most famous two-dimensional Gaussian field. It is the continuous-domain generalization of a family of independent and identically distributed Gaussian random variables (discrete Gaussian white noise). The white noise W is stationary and such that $\langle W, f \rangle$ and $\langle W, g \rangle$ are independent as soon as $\langle f, g \rangle = 0$. Observing W through a test function $f \in L_2(\mathbb{R}^2)$ gives a Gaussian random variable $\langle W, f \rangle$ with zero-mean and variance $\sigma^2 \|f\|_2^2$ [33]. We then call σ^2 the variance of W .

One can more generally consider random fields S such that $L\{S\} = W$ is a Gaussian white noise, where L is a linear differential operator. Since the effect of applying L is to whiten the field S , L is called the whitening operator of S . As developed more extensively in [33], one can deduce the expression of the variance of $\langle S, f \rangle$ from the variance of the white noise as follows. Consider a function $g \in L_2(\mathbb{R}^2)$ and set $f = L^*\{g\}$, with L^* the adjoint of L . Then, we have by duality that

$$\langle S, f \rangle = \langle S, L^*\{g\} \rangle = \langle L\{S\}, g \rangle = \langle W, g \rangle. \quad (28)$$

In particular, we deduce that $\langle S, f \rangle \sim \mathcal{N}(0, \sigma^2 \|g\|_2^2)$, which gives (11). In this case, $L = (-\Delta)^{\gamma/2}$, which is self-adjoint in the sense that $((-\Delta)^{\gamma/2})^* = (-\Delta)^{\gamma/2}$. We then have $\hat{f}(\boldsymbol{\omega}) = \|\boldsymbol{\omega}\|^\gamma \hat{g}(\boldsymbol{\omega})$. Hence,

$$\begin{aligned} \|\hat{g}\|_2^2 &= \frac{1}{2\pi} \|\hat{g}\|_2^2 = \frac{1}{2\pi} \int_{\mathbb{R}^2} \frac{|\hat{f}(\boldsymbol{\omega})|^2}{\|\boldsymbol{\omega}\|^{2\gamma}} d\boldsymbol{\omega} \\ &= \frac{1}{2\pi} \int_0^\infty r^{1-2\gamma} \int_0^{2\pi} |\hat{f}(r, \theta)|^2 d\theta dr \end{aligned} \quad (29)$$

implying (11).

B. Polar Decomposition of L_2 -functions

We provide here the proof of Proposition 1. We consider a function $f \in L_2(\mathbb{R}^2)$. For $r \geq 0$ fixed, the function $\theta \mapsto f(r, \theta)$ is in $L_2([0, 2\pi))$ and can therefore be decomposed in Fourier series. We denote by $\hat{f}_n(r)$ the complex Fourier coefficients, such that, for all $\theta \in [0, 2\pi)$,

$$f(r, \theta) = \sum_{n \in \mathbb{Z}} \hat{f}_n(r) e^{jn\theta}. \quad (30)$$

Using Parseval's relation and the orthogonality of the system $(\hat{f}_n(r) e^{jn\theta})_{n \in \mathbb{Z}}$, we have that

$$\begin{aligned} \|f\|_2^2 &= \frac{1}{2\pi} \|\hat{f}\|_2^2 = \frac{1}{2\pi} \int_0^\infty \int_0^{2\pi} |\hat{f}(r, \theta)|^2 r d\theta dr \\ &= \frac{1}{2\pi} \int_0^\infty \left(\int_0^{2\pi} \sum_{n, m \in \mathbb{Z}} \hat{f}_n(r) \overline{\hat{f}_m(r)} e^{j(n-m)\theta} d\theta \right) r dr \\ &= \int_0^\infty \sum_{n \in \mathbb{Z}} |\hat{f}_n(r)|^2 r dr = \sum_{n \in \mathbb{Z}} \|\hat{f}_n\|_2^2. \end{aligned}$$

This proves that f is square-integrable if and only if $\sum_{n \in \mathbb{Z}} \|\hat{f}_n\|_2^2 < \infty$. Finally, we remark that, for every $r \geq 0$,

$$\begin{aligned} \frac{1}{2\pi} \int_0^{2\pi} \hat{f}(r, \theta) e^{-jn\theta} d\theta &= \sum_{m \in \mathbb{Z}} \hat{f}_m(r) \frac{1}{2\pi} \int_0^{2\pi} e^{j(m-n)\theta} d\theta \\ &= \hat{f}_n(r), \end{aligned}$$

which proves (5) together with the fact that the decomposition is unique.

C. Optimal Steerable Filter: Without Whitening

This section is dedicated to the proof of Theorem 1. Using Proposition 1, we decompose the template in Fourier domain as $\hat{T}(r, \theta) = \sum_{n \in \mathbb{Z}} \hat{T}_n(r) e^{jn\theta}$. We set

$$P_H\{\hat{T}\}(r, \theta) = \sum_{n \in H} \hat{T}_n(r) e^{jn\theta} \quad (31)$$

where H is the finite set of harmonics. The operator P_H corresponds to the orthogonal projection onto the space of steerable filters with a set of harmonics H . Then, the orthogonality properties of the circular harmonics $e^{jn\theta}$ easily implies that $\langle \hat{f}, \hat{T} \rangle = \langle \hat{f}, P_H\{\hat{T}\} \rangle$ when \hat{f} is steerable with set of harmonics H . The Cauchy-Schwarz inequality now implies that $|\langle \hat{f}, P_H\{\hat{T}\} \rangle| \leq \|\hat{f}\|_2 \|P_H\{\hat{T}\}\|_2$. Putting things together, one therefore has

$$\begin{aligned} \text{SNR}(f) &= \frac{|\langle T, f \rangle|^2}{\|f\|_2^2} = \frac{|\langle \hat{T}, \hat{f} \rangle|^2}{\|\hat{f}\|_2^2} = \frac{|\langle P_H\{\hat{T}\}, \hat{f} \rangle|^2}{\|\hat{f}\|_2^2} \\ &\leq \|P_H\{\hat{T}\}\|_2^2. \end{aligned} \quad (32)$$

Moreover, the upper bound in (32), that does not depend on f , is reached if and only if \hat{f} is proportional to $P_H\{\hat{T}\}$ (equality case in the Cauchy-Schwarz inequality), as expected. Note that the above reasoning is valid because the function $P_H\{\hat{T}\}$ is itself steerable with the adequate set of harmonics.

D. Optimal Steerable Filter: With Whitening

The main idea is to reduce Proposition 2 to Theorem 1. The criterion (12) is optimized among the filters $f = (-\Delta)^{\gamma/2} g$ for some $g \in L_2(\mathbb{R}^2)$. For such filters, we have $\hat{f} = \|\cdot\|^\gamma \hat{g}$, implying that

$$\frac{|\langle \hat{T}, \hat{f} \rangle|^2}{\|\hat{g}\|_2^2} = \frac{|\langle \hat{T}, \|\cdot\|^\gamma \hat{g} \rangle|^2}{\|\hat{g}\|_2^2} = \frac{|\langle \|\cdot\|^\gamma \hat{T}, \hat{g} \rangle|^2}{\|\hat{g}\|_2^2}. \quad (33)$$

Therefore, f maximizes (12) if and only if g maximizes $\frac{|\langle \|\cdot\|^\gamma \hat{T}, \hat{g} \rangle|^2}{\|\hat{g}\|_2^2}$ among square integrable functions. The latter is equivalent, according to Theorem 1, to $\hat{g}(r, \theta) =$

$\sum_{n \in H} (\|\cdot\|^\gamma \widehat{T})_n(r) e^{jn\theta}$ where the $(\|\cdot\|^\gamma \widehat{T})_n$ are the Fourier radial profiles of $\|\cdot\|^\gamma \widehat{T}$. Because $\|\cdot\|^\gamma$ is isotropic, we easily get that $(\|\cdot\|^\gamma \widehat{T})_n(r) = r^\gamma \widehat{T}_n(r)$. Finally, f maximizes (12) if and only if

$$\widehat{f}(r, \theta) \propto r^\gamma \sum_{n \in H} r^\gamma \widehat{T}_n(r) e^{jn\theta} = r^{2\gamma} \sum_{n \in H} \widehat{T}_n(r) e^{jn\theta} \quad (34)$$

and (13) is proved.

E. Computing Radial B-spline Expansions

We here provide the proofs of Proposition 3 and Theorem 2. In the two cases, the main argument is the following classical result, that can be found for instance in [45].

Proposition 4: Assume that $(\varphi_n)_{n \in \mathbb{Z}}$ is a family of square integrable functions forming a Riesz basis; that is, satisfying

$$A \sum_{n \in \mathbb{Z}} c[n]^2 \leq \left\| \sum_{n \in \mathbb{Z}} c[n] \varphi_n \right\|_2^2 \leq B \sum_{n \in \mathbb{Z}} c[n]^2 \quad (35)$$

with $0 < A \leq B < \infty$. Then, the orthogonal projection onto the span V of the φ_n is of the form

$$P_V\{f\} = \sum_{n \in \mathbb{Z}} c[n] \varphi_n \quad (36)$$

where the sequence $c[n]$ satisfies the relation $G\{c\} = d$, with

$$G[n, m] = \langle \varphi_n, \varphi_m \rangle \quad \text{and} \quad d[n] = \langle f, \varphi_n \rangle. \quad (37)$$

The (infinite) matrix G is called the Gram matrix. Proposition 4 allows to express the expansion of functions in non-orthonormal basis from the quantities $\langle f, \varphi_n \rangle$.

We can now prove Proposition 3. The family $\left(\frac{1}{r_0} \beta(\cdot/r_0 - k)\right)_{k \in \mathbb{Z}}$ forms a Riesz basis of $L_2(\mathbb{R})$ [38], and this property is easily extended to the case of radial functions of $L_2(\mathbb{R}^2)$. Therefore, the coefficients $d[k]$ are given by (20) and the Gram matrix is given by

$$\begin{aligned} G[k, \ell] &= \left\langle \frac{1}{r_0} \beta\left(\frac{r}{r_0} - k\right), \frac{1}{r_0} \beta\left(\frac{r}{r_0} - \ell\right) \right\rangle \\ &= \int_{\mathbb{R}} \beta\left(\frac{r}{r_0} - k\right) \beta\left(\frac{r}{r_0} - \ell\right) \frac{r}{r_0} d\left(\frac{r}{r_0}\right) \\ &= \int_{\mathbb{R}} \beta(r) \beta(r - (\ell - k)) r dr, \end{aligned} \quad (38)$$

where we used the change of variable $r \leftarrow (r/r_0 - k)$. In particular, $G[k, \ell]$ does not depend on r_0 and only on the difference $(\ell - k)$. Denoting $g[k] = G[0, k]$, we hence have that $G\{c\} = g * c = d$, which is equivalent to (21) and proves Proposition 3.

We obtain Theorem 2 with the same arguments applied to the family $(\varphi_{n,k})_{n \in H, k \in \mathbb{Z}}$. We recall that two functions $\varphi_{n,k}$ and $\varphi_{m,\ell}$ are orthogonal as soon as $n \neq m$ since the circular harmonics are. Therefore, one can treat the problem independently for each harmonics and apply Proposition 3 on the Fourier radial profiles \widehat{T}_n of T .

For the last point, quadratic splines are known to well approximate functions from \mathbb{R} to \mathbb{R} up to an arbitrary precision [38]. This fact is easily adapted to the case of two-dimensional radial functions. We then deduce that, for each n , the orthogonal projection of \widehat{T}_n converges to \widehat{T}_n when the step size $r_0 \rightarrow 0$. Then, we remark, using the triangular inequality and the orthogonal relations between circular harmonics, that

$$\begin{aligned} \|\widehat{T} - P_{H, r_0}\{\widehat{T}\}\|_2 &\leq \|\widehat{T} - P_H\{\widehat{T}\}\|_2 + \|P_H\{\widehat{T}\} - P_{H, r_0}\{\widehat{T}\}\|_2 \\ &= \|\widehat{T} - P_H\{\widehat{T}\}\|_2 + \left(\sum_{n \in H} \|\widehat{T}_n - P_{r_0}\{\widehat{T}_n\}\|_2^2 \right)^{1/2} \end{aligned} \quad (39)$$

where P_{r_0} is given in (19). For H finite and large enough, the first quantity in (39) is arbitrarily small. Then, for such H , one can select r_0 such that $\|\widehat{T}_n - P_{r_0}\{\widehat{T}_n\}\|_2$ is arbitrarily small for each $n \in H$. Finally, one can approximate \widehat{T} with arbitrary precision for H large enough and r_0 small enough.

ACKNOWLEDGEMENTS

The authors are grateful to Emrah Bostan for his precious help regarding the statistical estimation of self-similar parameters. They also thank Daniel Sage for fruitful discussions.

REFERENCES

- [1] M. Sonka, V. Hlavac, and R. Boyle, *Image processing, analysis, and machine vision*. Cengage Learning, 2014.
- [2] R. M. Rangayyan, *Biomedical image analysis*. CRC press, 2004.
- [3] A. F. Frangi, W. J. Niessen, K. L. Vincken, and M. A. Viergever, "Multiscale vessel enhancement filtering," in *International Conference on Medical Image Computing and Computer-Assisted Intervention*, pp. 130–137, Springer, 1998.
- [4] A. Depeursinge, "Multiscale and multidirectional biomedical texture analysis," *Biomedical Texture Analysis: Fundamentals, Tools and Challenges*, p. 29, 2017.
- [5] A. Depeursinge, J. Fageot, and O. S. Al-Kadi, "Fundamentals of Texture Processing for Biomedical Image Analysis: A General Definition and Problem Formulation," in *Biomedical Texture Analysis: Fundamentals, Applications and Tools*, Elsevier-MICCAI Society Book series, pp. 1–27, Elsevier, 2017.
- [6] D. H. Ballard, "Generalizing the Hough transform to detect arbitrary shapes," *Pattern Recognition*, vol. 13, no. 2, pp. 111–122, 1981.
- [7] D. Marr and E. Hildreth, "Theory of edge detection," *Proceedings of the Royal Society of London B: Biological Sciences*, vol. 207, pp. 187–217, February 1980.
- [8] J. Canny, "A computational Approach to Edge Detection," *IEEE Transactions on Pattern Analysis and Machine Intelligence*, vol. 8, no. 6, pp. 679–698, 1986.
- [9] C. Harris and M. Stephens, "A Combined Corner and Edge Detection," in *Proceedings of The Fourth Alvey Vision Conference*, pp. 147–151, 1988.
- [10] W. Ouyang, F. Tombari, S. Mattoccia, L. D. Stefano, and W. K. Cham, "Performance Evaluation of Full Search Equivalent Pattern Matching Algorithms," *IEEE Transactions on Pattern Analysis and Machine Intelligence*, vol. 34, pp. 127–143, January 2012.
- [11] S. Korman, D. Reichman, G. Tsur, and S. Avidan, "Fast-Match: Fast Affine Template Matching," *International Journal of Computer Vision*, vol. 121, pp. 111–125, January 2017.
- [12] D. Marimon and T. Ebrahimi, "Efficient Rotation-Discriminative Template Matching," in *Progress in Pattern Recognition, Image Analysis and Applications* (L. Rueda, D. Mery, and J. Kittler, eds.), (Berlin, Heidelberg), pp. 221–230, Springer Berlin Heidelberg, 2007.
- [13] E. J. Bekkers, M. Loog, B. M. t. H. Romeny, and R. Duits, "Template Matching via Densities on the Roto-Translation Group," *IEEE Transactions on Pattern Analysis and Machine Intelligence*, vol. 40, no. 2, pp. 452–466, 2018.

- [14] E. Simoncelli and H. Farid, "Steerable wedge filters," in *Computer Vision, 1995. Proceedings., Fifth International Conference on*, pp. 189–194, IEEE, 1995.
- [15] K. Liu, Q. Wang, W. Driever, and O. Ronneberger, "2d/3d rotation-invariant detection using equivariant filters and kernel weighted mapping," in *IEEE Conference on Computer Vision and Pattern Recognition*, pp. 917–924, June 2012.
- [16] M. Muehlich, D. Friedrich, and A. Aach, "Design and implementation of multisteerable matched filters," *IEEE transactions on pattern analysis and machine intelligence*, vol. 34, no. 2, pp. 279–291, 2012.
- [17] Z. Püspöki, V. Uhlmann, C. Vonesch, and M. Unser, "Design of steerable wavelets to detect multifold junctions," *IEEE Transactions on Image Processing*, vol. 25, no. 2, pp. 643–657, 2016.
- [18] W. Freeman and E. Adelson, "The design and use of steerable filters," *IEEE Transactions on Pattern Analysis and Machine Intelligence*, vol. 13, no. 9, pp. 891–906, 1991.
- [19] M. Unser and N. Chenouard, "A unifying parametric framework for 2d steerable wavelet transforms," *SIAM Journal on Imaging Sciences*, vol. 6, no. 1, pp. 102–135, 2013.
- [20] Z. Püspöki and M. Unser, "Template-free wavelet-based detection of local symmetries," *IEEE Transactions on Image Processing*, vol. 24, no. 10, pp. 3009–3018, 2015.
- [21] O. Ronneberger, P. Fischer, and T. Brox, "U-Net: Convolutional Networks for Biomedical Image Segmentation," in *Medical Image Computing and Computer-Assisted Intervention – MICCAI 2015* (N. Navab, J. Hornegger, W. M. Wells, and A. F. Frangi, eds.), vol. 9351 of *Lecture Notes in Computer Science*, pp. 234–241, Springer International Publishing, 2015.
- [22] A. Esteva, B. Kuprel, R. A. Novoa, J. Ko, S. M. Swetter, H. M. Blau, and S. Thrun, "Dermatologist-level classification of skin cancer with deep neural networks," *Nature*, vol. 542, p. 115, January 2017.
- [23] P. Rajpurkar, J. Irvin, K. Zhu, B. Yang, H. Mehta, T. Duan, D. Ding, A. Bagul, C. Langlotz, K. Shpanskaya, M. P. Lungren, and A. Y. Ng, "CheXNet: Radiologist-Level Pneumonia Detection on Chest X-Rays with Deep Learning," *CoRR*, vol. abs/1711.05225, November 2017.
- [24] H. C. Shin, H. R. Roth, M. Gao, L. Lu, Z. Xu, I. Nogues, J. Yao, D. Mollura, and R. M. Summers, "Deep Convolutional Neural Networks for Computer-Aided Detection: CNN Architectures, Dataset Characteristics and Transfer Learning," *IEEE Transactions on Medical Imaging*, vol. 35, pp. 1285–1298, may 2016.
- [25] P. Y. Simard, D. Steinkraus, J. C. Platt, *et al.*, "Best practices for convolutional neural networks applied to visual document analysis," in *ICDAR*, vol. 3, pp. 958–962, 2003.
- [26] T. S. Cohen and M. Welling, "Group Equivariant Convolutional Networks," *CoRR*, vol. abs/1602.0, 2016.
- [27] M. Weiler, F. A. Hamprecht, and M. Storath, "Learning Steerable Filters for Rotation Equivariant CNNs," *CoRR*, vol. abs/1711.0, 2018.
- [28] X. Wang, Y. Peng, L. Lu, Z. Lu, M. Bagheri, and R. M. Summers, "ChestX-ray8: Hospital-scale Chest X-ray Database and Benchmarks on Weakly-Supervised Classification and Localization of Common Thorax Diseases," *CoRR*, vol. abs/1705.0, 2017.
- [29] H. V. Trees, *Detection, estimation, and modulation theory*. John Wiley & Sons, 2004.
- [30] A. Pentland, "Fractal-based description of natural scenes," *IEEE transactions on pattern analysis and machine intelligence*, no. 6, pp. 661–674, 1984.
- [31] P. Flandrin, "Wavelet analysis and synthesis of fractional Brownian motion," *IEEE Transactions on Information Theory*, vol. 38, no. 2, pp. 910–917, 1992.
- [32] D. Sage, F. Neumann, F. Hediger, S. Gasser, and M. Unser, "Automatic tracking of individual fluorescence particles: application to the study of chromosome dynamics," *IEEE Transactions on Image Processing*, vol. 14, no. 9, pp. 1372–1383, 2005.
- [33] M. Unser and P. D. Tafti, *An Introduction to Sparse Stochastic Processes*. Cambridge University Press, 2014.
- [34] P. Tafti and M. Unser, "Fractional Brownian vector fields," *Multiscale Modeling & Simulation*, vol. 8, no. 5, pp. 1645–1670, 2010.
- [35] A. Lodhia, S. Sheffield, X. Sun, and S. Watson, "Fractional Gaussian fields: A survey," *Probability Surveys*, vol. 13, pp. 1–56, 2016.
- [36] J. Fageot, E. Bostan, and M. Unser, "Wavelet statistics of sparse and self-similar images," *SIAM Journal on Imaging Sciences*, vol. 8, no. 4, pp. 2951–2975, 2015.
- [37] M. Unser, "Cardinal exponential splines: Part II—Think analog, act digital," *IEEE Transactions on Signal Processing*, vol. 53, no. 4, pp. 1439–1449, 2005.
- [38] M. Unser, "Splines: A perfect fit for signal and image processing," *IEEE Signal Processing Magazine*, vol. 16, no. 6, pp. 22–38, 1999.
- [39] C. d. Boor, K. Hollig, and S. Riemenschneider, "Fundamental solutions for multivariate difference equations," *American Journal of Mathematics*, vol. 111, no. 3, pp. pp. 403–415, 1989.
- [40] J. Fageot, M. Unser, and J. Ward, "Beyond Wiener's lemma: Nuclear convolution algebras and the inversion of digital filters," *arXiv preprint arXiv:1711.03999*, 2017.
- [41] S. R. P. Pavani, M. A. Thompson, J. S. Biteen, S. J. Lord, N. Liu, R. J. Twieg, R. Piestun, and W. E. Moerner, "Three-dimensional, single-molecule fluorescence imaging beyond the diffraction limit by using a double-helix point spread function," *Proceedings of the National Academy of Sciences*, vol. 106, no. 9, pp. 2995–2999, 2009.
- [42] D. G. Lowe, "Distinctive Image Features from Scale-Invariant Key-points," *International Journal of Computer Vision*, vol. 60, no. 2, pp. 91–110, 2004.
- [43] T. Lindeberg, "Dense scale selection over space, time, and space-time," *SIAM Journal on Imaging Sciences*, vol. 11, no. 1, pp. 407–441, 2018.
- [44] V. Uhlmann, J. Fageot, and M. Unser, "Hermite snakes with control of tangents," *IEEE Transactions on Image Processing*, vol. 25, no. 6, pp. 2803–2816, 2016.
- [45] A. Aldroubi and M. Unser, "Sampling procedures in function spaces and asymptotic equivalence with Shannon's sampling theory," *Numerical Functional Analysis and Optimization*, vol. 15, no. 1-2, pp. 1–21, 1994.